

Finite-size effects in the dynamics of neutrally buoyant particles in turbulent flow

By **HOLGER HOMANN**^{1,2} AND **JÉRÉMIE BEC**²

¹ Theoretische Physik I, Ruhr-Universität, 44780 Bochum, Germany

² Université de Nice-Sophia Antipolis, CNRS, Observatoire de la Côte d'Azur, Laboratoire Cassiopée, Bd. de l'Observatoire, 06300 Nice, France

(Received 20 July 2021)

The dynamics of neutrally buoyant particles transported by a turbulent flow is investigated for spherical particles with radii of the order of the Kolmogorov dissipative scale or larger. The pseudo-penalisation spectral method that has been proposed by Pasquetti *et al.* (2008) is adapted to integrate numerically the simultaneous dynamics of the particle and of the fluid. Such a method gives a unique handle on the limit of validity of point-particle approximations, which are generally used in applicative situations. Analytical predictions based on such models are compared to result of very well resolved direct numerical simulations. Evidence is obtained that Faxén corrections give dominant finite-size corrections to velocity and acceleration fluctuations for particle diameters up to four times the Kolmogorov scale. The dynamics of particles with larger diameters is dominated by inertial-range physics, and is consistent with predictions obtained from dimensional analysis.

1. Introduction

A large number of natural and engineering situations involves the transport of spherical finite-size particles by a fully developed turbulent flow. This includes the formation of planets in the early solar system, rain formation in clouds, the coexistence between several species of plankton, and many industrial settings encountered in chemistry and material processes. An important feature of such particles is that they do not follow exactly the fluid motion but have inertia, a property that leads to the development of inhomogeneities in their spatial distribution (see Squires & Eaton 1991; Balkovsky *et al.* 2001; Bec *et al.* 2007) or to the enhancement of the rate at which they collide (see Falkovich *et al.* 2002; Wilkinson *et al.* 2006; Zaichik *et al.* 2006; Bec *et al.* 2009). The modeling of such particles generally assumes that their diameter d_p is much smaller than the smallest active length-scale of the flow, that is the Kolmogorov scale η , so that they can be approximated by points (see Maxey & Riley 1983; Gatignol 1983). Modeling situations where $d_p \gtrsim \eta$ relies on the use of various empirical laws (as reviewed, for instance, in Clift *et al.* 1978). Generally such laws are obtained by considering a particle suspended in a mean laminar flow and interacting only through the turbulent wake that it creates, but not with a fully developed turbulent environment maintained by an external energy input.

Recent experimental developments have triggered a renewal of interest in the understanding and quantification of finite-size effects in the motion of particles in a turbulent flow (Qureshi *et al.* 2007; Volk *et al.* 2008; Xu & Bodenschatz 2008; Calzavarini *et al.* 2009). These works addressed in particular the problem of delimiting the domain of

validity of the point-particle models that are largely used in applicative fields, and to understand which corrective terms give dominant corrections. Such questions remain largely open because of the difficulty in constructing analytically the fluid flow perturbed by the presence of the spherical particle. In the following, we briefly review the equations that govern the coupled dynamics of the flow and the particle. In an incompressible fluid with kinematic viscosity ν and subject to an external volumic forcing strain tensor \mathbb{F} , the velocity field \mathbf{u} solves the Navier–Stokes equation

$$\partial_t \mathbf{u} + (\mathbf{u} \cdot \nabla) \mathbf{u} = -\frac{1}{\rho_f} \nabla p + \nu \nabla^2 \mathbf{u} + \nabla \cdot \mathbb{F}, \quad \nabla \cdot \mathbf{u} = 0, \quad (1.1)$$

which is supplemented by a non-slip boundary condition

$$\mathbf{u}(\mathbf{X}_p(t) + (d_p/2) \mathbf{n}, t) = \mathbf{V}_p(t) + \frac{d_p}{2} \boldsymbol{\Omega}_p(t) \times \mathbf{n}, \quad \forall \mathbf{n} : |\mathbf{n}| = 1 \quad (1.2)$$

at the surface $\partial\mathcal{B}$ of the spherical particle. $\mathbf{X}_p(t)$ denotes here the trajectory of the center of the particle, $\mathbf{V}_p(t)$ its translational velocity, and $\boldsymbol{\Omega}_p(t)$ its rotation rate. The motion of the particle is determined by Newton's second law

$$m_p \frac{d\mathbf{V}_p}{dt} = (m_p - m_f) \mathbf{g} + \int_{\mathcal{B}} \nabla \cdot \mathbb{T} d\mathcal{V} = (m_p - m_f) \mathbf{g} + \int_{\partial\mathcal{B}} \mathbb{T} \cdot d\mathcal{S} \quad (1.3)$$

where $m_p = (\pi/6)\rho_p d_p^3$ is the particle mass (with ρ_p its mass density), $m_f = (\pi/6)\rho_f d_p^3$ the mass of the displaced fluid, \mathbf{g} is the acceleration of gravity $\mathbb{T} = -p\mathbb{I}_3 + (\mu/2)(\nabla\mathbf{u} + \nabla\mathbf{u}^T) + \rho_f\mathbb{F}$ denotes the fluid stress tensor, \mathbb{I}_3 is the identity, and $\mu = \rho_f\nu$ the dynamic viscosity. In addition, the sphere rotation rate $\boldsymbol{\Omega}_p$ changes according to the conservation of angular momentum

$$\mathcal{I} \frac{d\boldsymbol{\Omega}_p}{dt} = \frac{m_p}{10} d_p^2 \frac{d\boldsymbol{\Omega}_p}{dt} = \int_{\partial\mathcal{B}} \mathbf{n} \times (\mathbb{T} \cdot d\mathcal{S}), \quad (1.4)$$

where \mathbf{n} denotes the outward pointing unit-vector normal to the surface and where we have assumed that the mass moment of inertia tensor \mathcal{I} is that of a uniform solid sphere. Solving the system (1.1)-(1.4) is a difficult task as it involves a nonlinear partial differential equation for the fluid, which is coupled to a moving boundary condition on the sphere. Analytical treatments of such a complex dynamics has only been done when neglecting nonlinearities in the flow motion at the scale of the particle, so that (1.1) reduces to the Stokes equation (this leads to the usual point-particle models).

This study focuses on neutrally buoyant particles, *i.e.* $\rho_p = \rho_f$. This case is of interest for applications to problems of plankton dynamics in the ocean or of some types of ice crystals in clouds. The goal is here to give a complete description of the dynamical properties of particles with sizes of the order of the Kolmogorov dissipative scale η . The paper is organised as follows. In §2, we consider the model given by the point particle approximation. We show that in the case of neutrally buoyant particles, first-order finite-size effects are not due to particle inertia but purely stem from Faxén corrections. They intervene in the particle dynamics as $(d_p/\lambda)^2$, where λ designates the Taylor micro-scale. These results are validated numerically in §3 thanks to the use of a new dynamical pseudo-penalisation technique that has the advantage of allowing one to use a spectral code in order to integrate the Navier–Stokes equation with the proper boundary conditions. We show that, both for velocity and acceleration statistics, finite-size effects become noticeable for $d_p \simeq 3\eta$ and that first-order Faxén corrections are relevant up to $d_p = 4\eta$. For $d_p \gtrsim 4\eta$, the particle dynamics is dominated by inertial-range physics. We also present results on acceleration time correlation that confirm this fact. Finally, §4 is dedicated to concluding remarks and prospectives.

2. Point-particle approximation

The derivation of point-particle models relies on the assumption that the perturbation of the surrounding flow by particles is well described by the Stokes equation (see Gatignol 1983; Maxey & Riley 1983; Auton *et al.* 1988). This assumption clearly requires that the particle Reynolds number defined with the velocity difference between the fluid and the particle is very small. The motion of the neutrally buoyant particle is then given by

$$\frac{d\mathbf{V}_p}{dt} = \mathbf{A}^\mathcal{V}(t) - \frac{12\nu}{d_p^2} (\mathbf{V}_p - \mathbf{U}^\mathcal{S}(t)) + \frac{6}{d_p} \sqrt{\frac{\nu}{\pi}} \int_{-\infty}^t \left(\mathbf{A}^\mathcal{V}(s) - \frac{d\mathbf{V}_p}{ds} \right) \frac{ds}{\sqrt{t-s}}, \quad (2.1)$$

where $\mathbf{U}^\mathcal{S}$ and $\mathbf{A}^\mathcal{V}$ account for Faxén corrections. They are averages of the fluid velocity over the surface and of the fluid acceleration over the volume of the particle, respectively:

$$\mathbf{U}^\mathcal{S}(t) = \frac{2}{\pi d_p^2} \int_{\partial\mathcal{B}} \mathbf{u}(\mathbf{x}, t) d\mathcal{S} \quad \text{and} \quad \mathbf{A}^\mathcal{V}(t) = \frac{6}{\pi d_p^3} \int_{\mathcal{B}} \frac{D\mathbf{u}}{Dt}(\mathbf{x}, t) d\mathcal{V}, \quad (2.2)$$

where $D/Dt = \partial_t + \mathbf{u} \cdot \nabla$ denotes the material derivative along fluid tracer trajectories. The various forcing terms in (2.1) are, in order of appearance, the combination of the inertia force exerted by the undisturbed flow and the added mass, the Stokes viscous drag, and the Basset–Boussinesq history force. In the limit when the particle size is much smaller than the Taylor micro-scale λ , a Taylor expansion of the fluid velocity in the vicinity of the particle center leads to

$$\begin{cases} \mathbf{U}^\mathcal{S}(t) = \mathbf{u}(\mathbf{X}_p, t) + \frac{1}{40} d_p^2 \nabla^2 \mathbf{u}(\mathbf{X}_p, t) + \mathcal{O}[(d_p/\lambda)^4], \\ \mathbf{A}^\mathcal{V}(t) = (D\mathbf{u}/Dt)(\mathbf{X}_p, t) + \frac{1}{24} d_p^2 (D\nabla^2 \mathbf{u}/Dt)(\mathbf{X}_p, t) + \mathcal{O}[(d_p/\lambda)^4]. \end{cases} \quad (2.3)$$

In the limit of particle diameters much smaller than the Kolmogorov scale η , the Basset–Boussinesq history force gives a contribution much smaller than the viscous drag and can thus be neglected to leading order. Hence, finite-size neutrally buoyant particles obey asymptotically the minimal model equation

$$\frac{d\mathbf{V}_p}{dt} = \frac{D\mathbf{u}}{Dt}(\mathbf{X}_p, t) - \frac{12\nu}{d_p^2} [\mathbf{V}_p - \mathbf{u}(\mathbf{X}_p, t)]. \quad (2.4)$$

Note that in this model, the particle size enters only the coefficient of the drag force. However, as it is now shown, such an effect is actually not sufficient to account for leading-order corrections due to the particle finite size. Indeed, following Babiano *et al.* (2000) and introducing the velocity difference between the particle and the fluid $\mathbf{W}(t) = \mathbf{V}_p(t) - \mathbf{u}(\mathbf{X}_p(t), t)$, one can easily check that

$$\frac{d\mathbf{W}}{dt} = -\mathbf{W} \cdot \nabla \mathbf{u}(\mathbf{X}_p(t), t) - \frac{12\nu}{d_p^2} \mathbf{W}. \quad (2.5)$$

This implies that $\mathbf{W}(t) = \exp(-12\nu t/d_p^2) \mathcal{T}\exp[-\int_0^t \nabla \mathbf{u}(\mathbf{X}_p(s), s) ds] \mathbf{W}(0)$, where $\mathcal{T}\exp$ denotes the time-ordered exponential. Hence the amplitude of the velocity difference grows exponentially at large time, *i.e.* $|\mathbf{W}(t)| \simeq |\mathbf{W}(0)| \exp[-(12\nu/d_p^2 + \lambda_3)t]$, where λ_3 is the smallest Lyapunov exponent associated to $\mathcal{T}\exp[-\int_0^t \nabla \mathbf{u}(\mathbf{X}_p(s), s) ds]$. Because of the fluid flow incompressibility implying a vanishing sum of the Lyapunov exponents, $\lambda_3 \leq 0$. However, when d_p is sufficiently small, *i.e.* when $d_p \leq \sqrt{12\nu/|\lambda_3|}$, the exponential growth rate of $|\mathbf{W}|$ is negative and the particle velocity relaxes to that of the fluid. Estimating the value of λ_3 requires in principle to evaluate the Lyapunov exponents associated to the fluid flow strain along particle trajectories. However, because of the exponential relaxation of the particle velocities to that of the fluid, these exponents

are exactly those computed along tracer trajectories. The latter have been evaluated in direct numerical simulations (see, *e.g.*, Bec *et al.* 2006) and, once normalised by the inverse of the Kolmogorov eddy turnover time τ_η , depend weakly upon the Reynolds number of the flow: for Re_λ varying from 65 to 185, one observes $\tau_\eta \lambda_3 = 0.190 \pm 2\%$. To summarise, this shows that the minimal model (2.4) exactly sticks to tracer dynamics for sizes smaller than a fixed threshold, *i.e.* for

$$\Phi = \frac{d_p}{\eta} \leq \Phi^* = \sqrt{\frac{12}{\tau_\eta \lambda_3}} \approx 8. \quad (2.6)$$

Hence, for $\Phi \leq \Phi^*$ finite-size effects are not related to inertia but can only stem from terms that were neglected in this model. This observation explain why neutrally buoyant particles whose dynamics is approximated by the point-particle model (2.4) do not display any clustering properties, as observed by Calzavarini *et al.* (2008).

Let us now estimate the contribution from terms that were neglected, namely from the Faxén corrections and the Basset-Boussinesq history term. For this, we follow the approach of Maxey (1987) developed for small Stokes numbers and write the following perturbative Ansatz $\mathbf{V}_p(t) = \mathbf{u}(\mathbf{X}_p(t), t) + (d_p/\lambda)^\alpha \mathbf{f}(t) + o[(d_p/\lambda)^\alpha]$, where the order α and the function \mathbf{f} are to be determined. Inserting this form in (2.1) and (2.3), one obtains that the first-order terms originate from Faxén corrections to the viscous drag, so that $\alpha = 2$ and

$$\mathbf{V}_p(t) = \mathbf{u}(\mathbf{X}_p(t), t) + \frac{d_p^2}{40} \nabla^2 \mathbf{u}(\mathbf{X}_p(t), t) + \mathcal{O}[(d_p/\lambda)^4]. \quad (2.7)$$

Note that the synthetic velocity field defined above is divergence-free, implying that no effect of particle preferential concentration can be detected with first-order corrections. This asymptotic form (2.7) implies that the particle velocity variance satisfies

$$\langle |\mathbf{V}_p|^2 \rangle - \langle |\mathbf{u}|^2 \rangle \simeq \frac{d_p^2}{20} \langle \mathbf{u} \cdot \nabla^2 \mathbf{u} \rangle = -\frac{d_p^2}{20} \frac{\varepsilon}{\nu} = -\frac{\langle |\mathbf{u}|^2 \rangle}{20} \left(\frac{d_p}{\lambda} \right)^2, \quad (2.8)$$

where ε is the mean turbulent rate of kinetic energy dissipation. As for the variance of particle acceleration, one obtains from the time derivative of (2.7)

$$\left\langle \left| \frac{d\mathbf{V}_p}{dt} \right|^2 \right\rangle - \left\langle \left| \frac{D\mathbf{u}}{Dt} \right|^2 \right\rangle \simeq -\frac{d_p^2}{20} \left\langle \left\| \frac{D\nabla \mathbf{u}}{Dt} \right\|^2 \right\rangle = -\frac{d_p^2}{20} \langle (\nabla^2 p)^2 + \nu^2 \|\nabla^2 \nabla \mathbf{u}\|^2 \rangle, \quad (2.9)$$

where $\|\cdot\|$ denotes the tensorial Frobenius norm, *i.e.* $\|\mathbf{M}\|^2 = \text{trace}(\mathbf{M}^\top \mathbf{M})$. Hence we expect at small diameters that finite-size effects materialise as a falloff of the two above-mentioned dynamical properties of particles that behave quadratically as a function of the particle diameter with a coefficient given by Eulerian averaged quantities.

3. Numerical results using a pseudo-penalisation method

In order to assess numerically the effect of the particles' finite size on their dynamics, a pseudo-spectral code has been adapted to non-trivial geometries by using a pseudo-penalisation strategy. The purely spectral part of the parallel code LaTu, which was already used to investigate Lagrangian turbulence by Homann *et al.* (2007), solves accurately the incompressible Navier-Stokes equations. This method treats the evolution of the fluid velocity field in Fourier space and computes convolutions arising from the non-linear terms in physical space. The Fourier transformations are performed by the

Re_λ	u_{rms}	ε	ν	δx	δt	η	τ_η	L	T_L	N^3
32	0.17	$4.5 \cdot 10^{-3}$	$3 \cdot 10^{-3}$	$1.23 \cdot 10^{-2}$	$8 \cdot 10^{-3}$	$5 \cdot 10^{-2}$	0.8	1.2	6.5	512^3

TABLE 1. Parameters of the numerical simulations. $Re_\lambda = \sqrt{15u_{\text{rms}}L/\nu}$: Taylor-Reynolds number, u_{rms} : root-mean-square velocity, ε : mean kinetic energy dissipation rate, ν : kinematic viscosity, δx : grid-spacing, δt : time step, $\eta = (\nu^3/\varepsilon)^{1/4}$: Kolmogorov dissipation length scale, $\tau_\eta = (\nu/\varepsilon)^{1/2}$: Kolmogorov time scale, $L = (2/3E)^{3/2}/\varepsilon$: integral scale, $T_L = L/u_{\text{rms}}$: large-eddy turnover time, N^3 : number of collocation points.

P3DFFT-library.† The domain is a triple-periodic cube. This method allows for high accuracy, precise control of the physical parameters and numerical efficiency. In order to maintain a statistically steady state we force the flow by prescribing the energy content of the Fourier vectors with moduli 1 and 2. The energy content of each of these two shells is kept constant while the individual amplitudes and phases are evolved piecewise linearly in time between several random configurations separated by a time $10T_L$. The advantages of such a forcing are two-fold: it allows one to achieve a statistically isotropic large-scale flow and limits the fluctuations to only approximately 10% of the mean. The turbulent characteristics of the flow generated in this way are summarised in Tab. 1.

In order to impose the no-slip boundary condition on the surface of the spherical particle, we follow Pasquetti *et al.* (2008) and use a pseudo-penalisation method, which consists in imposing a strong drag to the fluid velocity at the particle location, so that it relaxes quickly to the particle solid motion. The hydrodynamical forces acting on the particle are computed by a Riemann approximation of the integrals appearing in (1.3) and (1.4) on a homogeneous grid of discrete points located on the surface of the sphere. The value of pressure at these points is computed by tri-cubic interpolation. The surface integral of the fluid velocity gradient is computed from evaluating the average velocity on spherical shells surrounding the particle. At the moment, the simulations are limited to a single particle in order to prevent the individual dynamical properties from being contaminated by particle-particle hydrodynamical interactions. Notice however that the code is very well adapted to situations involving several particles. Because only a single isolated particle is considered in the flow, the statistical convergence of particle-related quantities requires to perform averages over very long times. Each simulation for a single value of the particle diameter required to integrate the flow over more than three hundreds large-eddy turnover times. Eight different particle diameters d_p are considered within the range 2η to 14η . As the pseudo-penalisation technique requires several grid-points inside the object in order to correctly impose the boundary conditions, the Kolmogorov dissipative scale η is resolved with four grid points. This requires the use of double floating point precision. Because of the large spatial resolution and the long time integration which are required, the simulations are very computationally demanding: this work took approximately four millions of single processor CPU hours. Figure 1 (Left) shows the typical vorticity field in a cut-plane passing through the center of the particle. Note that the signature of a turbulent wake is visible on the right-hand side of the particle.

To benchmark these simulations, a run with the same parameters as those shown in Tab. 1 but without any finite-size particle has been performed. In this simulation, we have integrated the motion of passive point particles with a dynamics obeying (2.4) and of passive tracers. It is worthwhile mentioning here that turbulent fluid statistical quantities are observed not to depend on the presence of a particle, up to the statistical

† Parallel 3D Fast Fourier Transforms (P3DFFT), <http://www.sdsc.edu/us/resources/p3dfft>

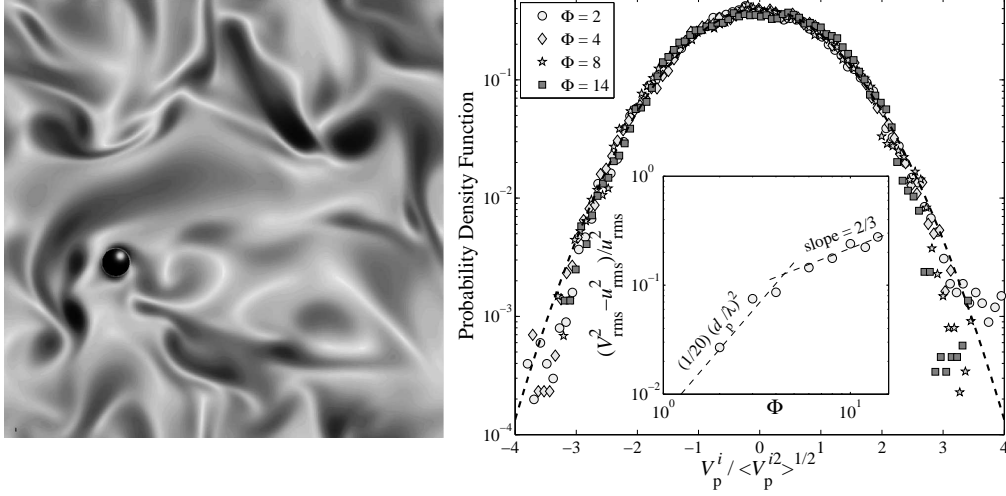


FIGURE 1. *Left*: modulus of the vorticity in a slice of the domain that is passing through the center of the embedded particle (dark = high vorticity, light = low vorticity); the particle diameter is here $d_p = 8\eta$. *Right*: normalised probability density function of the particle velocity for various particles sizes, as labeled; the bold dash line corresponds to a Gaussian distribution. Inset: deviation of the particle velocity variance $V_{\text{rms}}^2 = \langle |\mathbf{V}_p|^2 \rangle$ from the fluid value, as a function of the non-dimensionalised particle diameter $\Phi = d_p/\eta$; the two dashed line represent the deviation (2.8) from the fluid root-mean square velocity that is expected to stem from Faxén corrections and a behaviour $\propto d_p^{2/3}$, respectively .

fluctuations due to finite time averages. The particle-free simulation serves thus as a reference to estimate tracer statistics and Eulerian averages.

Figure 1 (Right) shows the probability density function (PDF) of the particle velocity components for various particle diameters. Once normalised by their standard deviations, these PDFs almost collapse on top of each other and deviate very weakly from a Gaussian distribution. The measured variance of the particle velocity that is represented in the inset, decreases as a function of the particle size. For small diameters, *i.e.* for $\Phi = d_p/\eta \lesssim 4$, the behaviour of the particle velocity variance is very well described by the prediction (2.8) obtained from Faxén corrections. For $\Phi \gtrsim 4$, the deviation from the fluid velocity variance behaves as $\Phi^{2/3}$. This power-law is dimensionally compatible with Kolmogorov 1941 scaling and indicates that particles with such diameters respond to the inertial-range physics of turbulence. Noticeably, in the low-Reynolds-number flow that we are considering here, there is no inertial range in the sense usually defined through velocity scaling properties. Hence it seems that particle dynamical properties are much more amenable to dimensional estimates than fluid turbulent quantities.

We next turn to particle acceleration statistics. Figure 2 (Left) represents the componentwise normalised variance of the particle acceleration $a_0 = \langle (dV_p^i/dt)^2 \rangle \epsilon^{-4/3} \eta^{2/3}$ as a function of the non-dimensionalised diameter $\Phi = d_p/\eta$, both for the real particles as well as for the minimal point model (2.4). For real spherical particles, one distinguishes, as in the case of velocity variance, between two behaviours. When $\Phi = d_p/\eta \lesssim 4$, finite-size effects in the acceleration variance are very well captured by Faxén corrections and are very close to the prediction (2.9). Note that, thanks to their isotropic form, the sub-leading terms appearing in (2.9) could be evaluated here through the pressure and velocity spectra. When $\Phi \gtrsim 4$, an inertial-range behaviour with $a_0 \propto d_p^{-4/3}$ is attained. As argued by Qureshi *et al.* (2007), the variance of finite-size particle acceleration is re-

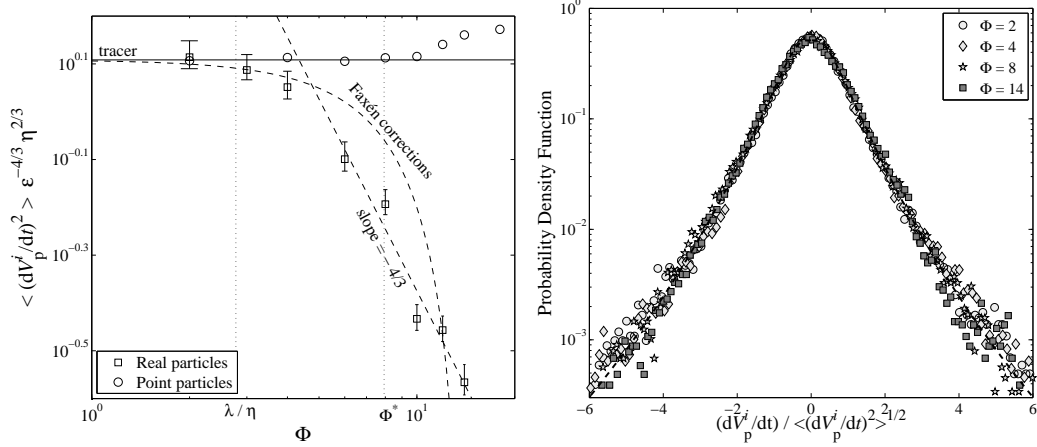


FIGURE 2. *Left*: acceleration variance of real spheres and of point particles as a function of the non-dimensionalised particle diameter $\Phi = d_p/\eta$; error bars correspond to an estimation of the standard deviations. The two dotted vertical line indicate the Taylor micro-scale λ and the critical value (2.6) above which point particles deviate from fluid tracers. The dashed curve corresponds to the behaviour (2.9) predicted from Faxén corrections. *Right*: normalised probability density function of the component-wise particle acceleration for various particle diameter, as labeled. The bold dashed line on which data almost collapse corresponds to the log-normal fit (3.1) of experimental data proposed by Qureshi *et al.* (2007).

lated to that of the fluid pressure integrated over a sphere of diameter d_p . The power $-4/3$ that is observed here differs from the value $-2/3$, which was measured by Qureshi *et al.* However, as already stressed for instance in Bec *et al.* (2007), pressure scaling in low Reynolds number flows is often dominated by sweeping, leading to a behaviour of the pressure increments $|p(x + \ell) - p(x)| \sim \ell^{1/3}$. While no scaling of pressure can be detected in the present simulations, the robustly observed $-4/3$ law can be explained with such a sweeping-dominated pressure spectrum. Another observation is that numerics confirm the presence of the threshold (2.6) predicted in the previous section for the minimal point particle model: indeed the numerical integration of point particles obeying (2.4) shows that when $\Phi < 8$, the acceleration variance of the latter is undistinguishable from that of tracers. For $\Phi > 8$, the point particle model gives an enhancement of acceleration, which is incompatible with measurements done with real particles at the Reynolds number considered here. This stresses the irrelevance of such a model in the case of neutrally buoyant particles. Note finally that in the case of tracers, the constant a_0 is known to show a Reynolds number dependence $a_0 \propto R_\lambda^{1/2}$ (see, *e.g.*, Voth *et al.* 2002). The measured value of approximately 1.3 is in good agreement with the value that was measured experimentally by Qureshi *et al.* (2007).

Figure 2 (Right) represents the PDF of acceleration components normalised to unity variances for various values of the particle diameter. As already stressed in Qureshi *et al.* (2007), the dependence upon $\Phi = d_p/\eta$ is very weak. Data can be fitted by the function

$$p(a) = \left[\exp(3s^2/2) / (4\sqrt{3}) \right] \left\{ 1 - \operatorname{erf} \left[\left(\ln |x/\sqrt{3}| + 2s^2 \right) / (\sqrt{2}s) \right] \right\}, \quad (3.1)$$

which was proposed by Mordant *et al.* (2004) for the acceleration PDF of fluid tracers. Numerical results almost collapse to such a distribution with a value of the parameter $s = 0.62$, as observed by Qureshi *et al.* (2007).

Other measurements relate to two-time statistical properties of particles. Figure 3

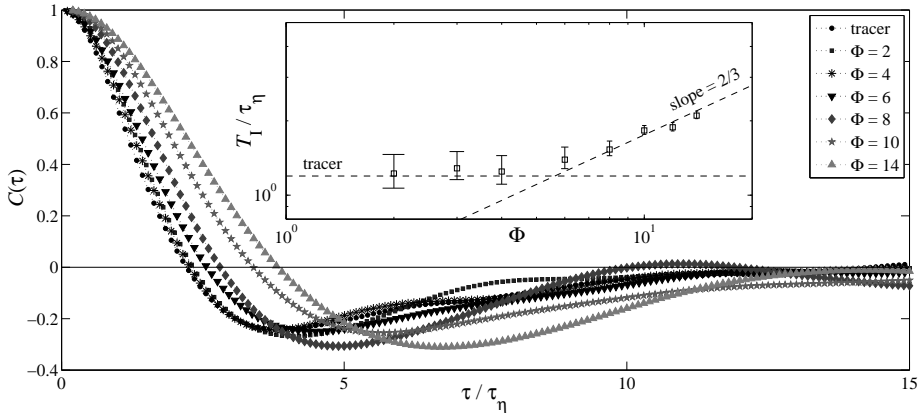


FIGURE 3. Component-wise acceleration time correlation $C(\tau)$ defined in (3.2) for various particle sizes, as labeled. Inset: integral correlation time T_I defined from (3.3) as a function of the non-dimensionalised particle diameter $\Phi = d_p/\eta$.

represents the acceleration time correlation

$$C(\tau) \equiv \left\langle \frac{dV_p^i}{dt}(t+\tau) \frac{dV_p^i}{dt}(t) \right\rangle / \left\langle \left(\frac{dV_p^i}{dt} \right)^2 \right\rangle \quad (3.2)$$

as a function of the time lag τ for various values of the particle diameter. The numerical measurements reported here are in good agreement with the results of Calzavarini *et al.* (2009). Surprisingly one observes that $C(\tau)$ deviates only very weakly from the tracer acceleration temporal correlation for diameters less than 4η , that is when Faxén corrections are expected to be of relevance to capture first-order finite-size effects. This behaviour is even clearer when looking at the diameter dependence of the correlation time for particle acceleration. For this we follow Calzavarini *et al.* (2009) and introduce the integral time

$$T_I \equiv \int_0^{T_0} C(\tau) d\tau, \quad (3.3)$$

where T_0 is the first zero-crossing time. The inset of Fig. 3 represents T_I/τ_η as a function of $\Phi = d_p/\eta$. When $\Phi \lesssim 4$, this integral correlation time is, up to numerical errors, undistinguishable from the value obtained for tracers. When $\Phi \gtrsim 4$, the correlation time increases much faster as a function of Φ and follows approximately the power-law behaviour $T_I \sim \Phi^{2/3}$. This indicates again that turbulent inertial physics is pulling strings at such values of the particle diameter, and that the relevant time scale is then given by the eddy turnover time $\sim \varepsilon^{-1/3} d_p^{2/3}$ associated to the particle size.

4. Concluding remarks

In this paper it is shown that first-order finite-size corrections to the dynamics of neutrally buoyant particles are due to Faxén terms and not to particle inertia. This leads to several predictions on turbulent velocity and acceleration second-order statistics. Using a pseudo-penalisation spectral method, these predictions have been confirmed numerically for particles with diameters d_p up to 4η . Higher-order statistics of velocity and acceleration seem much less sensitive to the finiteness of the particle sizes, since numerical observation suggest that, once normalised to unit variance, their PDFs collapse on top of each other for various values of the particle diameter.

The irrelevance of particle inertia with respect to Faxén terms at small particle diameters has noticeable consequences. First, it implies that the particle dynamics is very well approximated by the advection by a synthetic flow, which is incompressible to both the leading and the first orders. This means that the effect of preferential concentration onto the dynamics of neutrally buoyant particles is very weak. Secondly, such an observation clearly questions the relevance of inertial-particle models for density contrasts between the particle and the fluid that are close to one. A third consequence is related to the fact that corrective terms apply when the particle diameter is much smaller than the Taylor micro-scale λ rather than the Kolmogorov dissipative scale η . This fact might partly explain the difficulties in matching experiments and numerical model including Faxén corrections (see, *e.g.*, Calzavarini *et al.* 2009).

For particle diameters larger than $\approx 4\eta$, inertial-range physics comes into play. A striking observation is the relevance of the dimensional estimates that are given by Kolmogorov 1941 theory, even when the fluid flow Reynolds number is so low that no scaling range can be observed for Eulerian velocity statistics. Understanding the reasons of such a behaviour requires to investigate in a more systematic manner the dynamics of particles with inertial-range sizes in fully developed turbulent flow. Applying the pseudo-penalisation method to larger particles and higher fluid flow Reynolds numbers is the subject of on-going work that is mainly focusing on describing the flow modification induced by the presence of the spherical particle.

ACKNOWLEDGMENTS. This study benefited from fruitful discussions with M. Bourgoïn, E. Calzavarini, R. Pasquetti, and Y. Ponty. This research was supported by the Agence Nationale de la Recherche under grant No. BLAN07-1_192604. During his stay in Nice, H. Homann benefited from a grant of the DAAD. Access to the IBM BlueGene/P computer JUGENE at the FZ Jülich was made available through project HBO22. Part of the computations were performed on the “mésocentre de calcul SIGAMM” and using HPC resources from GENCI-IDRIS (Grant 2009-i2009026174).

REFERENCES

- AUTON, T., HUNT, J. & PRUD’HOMME, M. 1988 The force exerted on a body in inviscid unsteady non-uniform rotational flow. *J. Fluid Mech.* **197**, 241–257.
- BABIANO, A., CARTWRIGHT, J.H.E., PIRO, O. & PROVENZALE, A. 2000 Dynamics of a small neutrally buoyant sphere in a fluid and targeting in Hamiltonian systems. *Phys. Rev. Lett.* **84**, 5764–5768.
- BALKOVSKY, E., FALKOVICH, G. & FOUXON, A. 2001 Intermittent distribution of inertial particles in turbulent flows. *Phys. Rev. Lett.* **86**, 2790–2793.
- BEC, J., BIFERALE, L., CENCINI, M., LANOTTE, A.S., MUSACCHIO, S. & TOSCHI, F. 2007 Heavy particle concentration in turbulence at dissipative and inertial scales. *Phys. Rev. Lett.* **98**, 84502.
- BEC, J., BIFERALE, L., CENCINI, M., LANOTTE, A.S. & TOSCHI, F. 2009 Intermittency in the velocity distribution of heavy particles in turbulence. Preprint arXiv:0905.1192.
- BEC, J., BOFFETTA, G., BIFERALE, L., CENCINI, M., MUSACCHIO, S. & TOSCHI, F. 2006 Lyapunov exponents of heavy particles in turbulence. *Phys. Fluids* **18**, 091702.
- CALZAVARINI, E., KERSCHER, M., LOHSE, D. & TOSCHI, F. 2008 Dimensionality and morphology of particle and bubble clusters in turbulent flow. *J. Fluid. Mech.* **607**, 13–24.
- CALZAVARINI, E., VOLK, R., BOURGOÏN, M., E., LÉVÊQUE, PINTON, J.-F. & TOSCHI, F. 2009 Acceleration statistics of finite-sized particles in turbulent flow : The role of Faxén forces. *J. Fluid. Mech.* **630**, 179–189.
- CLIFT, R., GRACE, J.R. & WEBER, M.E. 1978 *Bubbles, drops and particles*. London: Academic Press.
- FALKOVICH, G., FOUXON, A. & STEPANOV, M.G. 2002 Acceleration of rain initiation by cloud turbulence. *Nature* **419**, 151–154.

- GATIGNOL, R. 1983 The Faxén formulae for a rigid sphere in an unsteady non-uniform Stokes flow. *J. Méc. Théor. Appl.* **1**, 143–160.
- HOMANN, H., GRAUER, R., BUSSE, A. & MÜLLER, W.C. 2007 Lagrangian Statistics of Navier-Stokes and MHD Turbulence. *J. Plasma Phys.* **73**, 821–830.
- MAXEY, M.R. 1987 The gravitational settling of aerosol particles in homogeneous turbulence and random flow fields. *J. Fluid Mech.* **174**, 441–465.
- MAXEY, M.R. & RILEY, J.J. 1983 Equation of motion for a small rigid sphere in a nonuniform flow. *Phys. Fluids* **26**, 883–889.
- MORDANT, N., CRAWFORD, A.M. & BODENSCHATZ, E. 2004 Three-dimensional structure of the Lagrangian acceleration in turbulent flows. *Phys. Rev. Lett.* **93**, 214501.
- PASQUETTI, R., BWEMBA, R. & COUSIN, L. 2008 A pseudo-penalization method for high Reynolds number unsteady flows. *Appl. Numer. Math.* **58** (7), 946–954.
- QURESHI, N.N., BOURGOIN, M., BAUDET, C., CARTELLIER, A. & GAGNE, Y. 2007 Turbulent transport of material particles: an experimental study of finite size effects. *Phys. Rev. Lett.* **99**, 184502.
- SQUIRES, K.D. & EATON, J.K. 1991 Preferential concentration of particles by turbulence. *Phys. Fluids A* **3**, 1169–1178.
- VOLK, R., CALZAVARINI, E., VERHILLE, G., LOHSE, D., MORDANT, N., PINTON, J.-F. & TOSCHI, F. 2008 Acceleration of heavy and light particles in turbulence: Comparison between experiments and direct numerical simulations. *Physica D* **237**, 2084–2089.
- VOTH, G.A., LA PORTA, A., CRAWFORD, A.M. & BODENSCHATZ, E. 2002 Measurement of particle accelerations in fully developed turbulence. *J. Fluid Mech.* **469**, 121–160.
- WILKINSON, M., MEHLIG, B. & V., BEZUGLYY 2006 Caustic activation of rain showers. *Phys. Rev. Lett.* **97**, 048501.
- XU, H. & BODENSCHATZ, E. 2008 Motion of inertial particles with sizes larger than Kolmogorov scales in turbulent flows. *Physica D* **237**, 2095–2100.
- ZACHNIK, L., SIMONIN, O. & ALIPCHENKOV, V. 2006 Collision rates of bidisperse inertial particles in isotropic turbulence. *Phys. Fluids* **18**, 035110.